Title

Novel factor in olfactory ensheathing cell-astrocyte crosstalk: Anti-inflammatory protein α-crystallin B

Journal

Glia, 69(4)

ISSN

0894-1491

Authors

Saglam, Aybike
Calof, Anne L
Wray, Susan

Publication Date

2021-04-01

DOI

10.1002/glia.23946

Peer reviewed

HHS Public Access

Author manuscript

Glia. Author manuscript; available in PMC 2022 September 13.

Published in final edited form as:

Glia. 2021 April ; 69(4): 1022–1036. doi:10.1002/glia.23946.

Novel factor in olfactory ensheathing cell-astrocyte crosstalk: Anti-inflammatory protein α-crystallin B

Aybike Saglam[1,2], **Anne L. Calof**[3], **Susan Wray**[1]

[1]Cellular & Developmental Neurobiology Section, NINDS, NIH, Bethesda, Maryland

[2]Program in Neuroscience & Cognitive Science, University of Maryland, College Park, Maryland

[3]Department of Anatomy & Neurobiology and the Center for Complex Biological Systems, University of California, Irvine, California

Abstract

Astrocytes are key players in CNS neuroinflammation and neuroregeneration that may help or hinder recovery, depending on the context of the injury. Although pro-inflammatory factors that promote astrocyte-mediated neurotoxicity have been shown to be secreted by reactive microglia, anti-inflammatory factors that suppress astrocyte activation are not well-characterized. Olfactory ensheathing cells (OECs), glial cells that wrap axons of olfactory sensory neurons, have been shown to moderate astrocyte reactivity, creating an environment conducive to regeneration. Similarly, astrocytes cultured in medium conditioned by cultured OECs (OEC-CM) show reduced nuclear translocation of nuclear factor kappa-B (NFκB), a pro-inflammatory protein that induces neurotoxic reactivity in astrocytes. In this study, we screened primary and immortalized OEC lines to identify these factors and discovered that Alpha B-crystallin (CryAB), an anti-inflammatory protein, is secreted by OECs via exosomes, coordinating an intercellular immune response. Our results showed that: (a) OEC exosomes block nuclear NFκB translocation in astrocytes while exosomes from CryAB-null OECs could not; (b) OEC exosomes could be taken up by astrocytes, and (c) CryAB treatment suppressed neurotoxicity-associated astrocyte transcripts. Our results indicate CryAB, as well as other factors secreted by OECs, are potential agents that can ameliorate, or even reverse, the growth-inhibitory environment created by neurotoxic reactive astrocytes following CNS injuries.

Keywords

alpha-crystallin B (CryAB); astrocyte; exosome; neuroinflammation; neurotoxicity; nuclear factor kappa B (NFκB); olfactory ensheathing cells (OECs)

Correspondence Susan Wray, Cellular & Developmental, Neurobiology Section, NINDS, NIH, Bethesda, MD. wrays@ninds.nih.gov.

AUTHOR CONTRIBUTIONS

Aybike Saglam and Susan Wray designed the research. Aybike Saglam performed the experiments. Aybike Saglam analyzed the data and Aybike Saglam, Anne L. Calof, and Susan Wray wrote the manuscript.

SUPPORTING INFORMATION

Additional supporting information may be found online in the Supporting Information section at the end of this article.

1 | INTRODUCTION

Damage to the central nervous system (CNS) provokes morphological and molecular changes in astrocytes, causing them to become “reactive astrocytes” (Liddelow & Barres, 2017). These reactive cells play positive roles during CNS injury, such as confining inflammation by surrounding the damaged tissue and creating a barrier between it and uninjured tissues (Silver, Schwab, & Popovich, 2015). However, chronic inflammation can lead to sustained and/or excessive astrocyte reactivity, which is neurotoxic and deleterious to functional recovery (Sofroniew & Vinters, 2010). A better understanding of the molecular mechanisms that govern astrocyte reactivity would therefore be helpful to create environments conducive to regeneration following CNS injury.

Until recently, reactive astrocytes were characterized by increased expression of intermediate filament proteins such as GFAP (Glial Fibrillary Acidic Protein), vimentin, and nestin (summarized in Liddelow & Barres, 2017). However, it is now apparent that these are not the most informative markers to evaluate the outcome of astrocyte reactivity, since their upregulation does not distinguish between different types of reactivity (Liddelow et al., 2017). Nuclear factor-κB (NFκB) activation is one of the early indicators and regulators of neurotoxic-astrocyte reactivity (Giovannoni & Quintana, 2020; Liddelow & Barres, 2017), yet the increase in NFκB transcription is transient (Liu, Zhang, Joo, & Sun, 2017). Fortunately, transcriptomic studies identified transcripts that are specifically upregulated in neuroinflammatory/neurotoxic astrocytes, such as complement component C3 (Liddelow et al., 2017).

The mammalian olfactory system shows robust neurogenesis throughout life. Data suggest that both neural niche signals and the surrounding glia, including olfactory ensheathing cells (OECs), give the olfactory mucosa this unique capability (Li, Field, & Raisman, 2005; Roet & Verhaagen, 2014). Several groups have transplanted OECs into CNS injury sites, and observed improved axonal regeneration (Imaizumi, Lankford, Burton, Fodor, & Kocsis, 2000; Li, Field, & Raisman, 1997), functional recovery (Johansson, Lee, Olson, & Spenger, 2005), reduced astrogliosis (Ramer et al., 2004), and an attenuated hostile astrocyte response (Lakatos, Barnett, & Franklin, 2003; summarized in Roet & Verhaagen, 2014). Moreover, factors secreted by OECs have been shown to moderate astrocyte reactivity, at least insofar as their presence results in reductions in GFAP expression and nuclear translocation of pro-inflammatory transcription factor NFκB (Chuah, Hale, & West, 2011; O’Toole, West, & Chuah, 2007). However, the molecular pathways for OEC-astrocyte crosstalk are understudied. Identification of molecules secreted by OECs, which moderate neurotoxic astrocyte reactivity, should lead not only to a better understanding of the crosstalk between astrocytes and OECs; it may also be used to develop strategies to beneficially manipulate astrocyte reactivity in CNS disorders in a context-dependent manner and replace the use of OECs for therapeutic transplantation.

To identify such molecules, this study used lipopolysaccharide (LPS)-treated astrocytes, a model for neurotoxic reactive astrocytes, and assessed conditioned medium (CM) from immortalized clonal mouse OEC cell lines (Calof & Guevara, 1993). Nuclear NFκB translocation in astrocytes was measured to determine if CM from these cell lines could

mimic primary OEC-CM, which blocked the LPS pro-inflammatory response in astrocytes. Two immortalized cell lines were chosen for further study: one whose CM mimicked the effect of primary OECs (positive control); and a second, whose CM did not block the LPS response in astrocytes (negative control). These two cell lines and primary OECs were challenged with LPS, and the conditioned media screened by mass spectrometry. Using this strategy, the heat-shock protein CryAB (D'Agostino et al., 2013) was identified. Subsequent experiments showed that: (a) CryAB is secreted by OECs via exosomes; (b) exogenous CryAB suppressed LPS-induced astrocyte reactivity; (c) exosomes containing CryAB are taken up by astrocytes; and (d) unlike wildtype (WT) OEC-exosomes, *CryAB*-null (*CryAB*$^{-/-}$) OEC exosomes fail to suppress LPS-induced astrocyte reactivity measured by nuclear NFκB translocation. Finally, examination of transcripts that are associated with neurotoxic-reactive astrocytes (Liddelow et al., 2017) revealed that either exogenous CryAB or OEC-CM can suppress expression of several of these transcripts. Our data indicate that CryAB secreted by OECs, via exosomes, is an important factor for OEC-astrocyte crosstalk that can block astrocytes from becoming neurotoxic cells. Ultimately, mimicking appropriate astrocyte-OEC crosstalk in vivo may contribute to an environment conducive to regeneration following a broad range of CNS injuries.

2 | MATERIALS AND METHODS

2.1 | Mice

All mice were maintained, and all animal handling procedures were performed according to protocols approved by the National Institutes of Health NINDS Institutional Animal Care and Use Committee. *CryAB*-null (*CryAB*$^{Del[9Hspb2\text{-}Cryab]1Wawr}$, henceforth referred to as *CryAB*$^{-/-}$) mice (Brady et al., 2001) were obtained as homozygous sperm, revived by IVF using eggs from C57bl6/N mice (Jackson Laboratory), and resulting heterozygotes intercrossed to obtain *CryAB*$^{-/-}$ and *CryAB*$^{+/+}$ (wildtype, WT) lines, which were used as the source for OEC primary cultures (see below). Mice were genotyped using a three-primer PCR protocol: 5′-TAGCTTAATAATCTGGGCCA-3′, 5′GGAGTTCCACAGGAAGT-ACC-3′, and 5′-TGGAAGGATTGGAGCTACGG-3′ primers were used in 4:1:1 M ratio. Amplification was performed for 40 cycles at 94°C for 15 s, 62°C for 30 s, and 72°C at 1 min. PCR produced a 310-bp product for the WT allele and a 600-bp product for the null allele.

2.2 | Cell culture and reagents

Primary cultures of OECs were generated as described previously (Dairaghi et al., 2018). Briefly, olfactory bulbs (OB) of postnatal (PN) day 0–7 mice were collected and placed in an enzyme mix (previously used to isolate OECs from olfactory epithelium [OE] and OB): 300 μg/ml hyaluronidase (Sigma, Cat# H3631, St. Louis, MO), 30 U/ml dispase I (Sigma, Cat# D4818), 1.2 mg/ml collagenase type 4 (Worthington, Cat# 43E14231, Lakewood, NJ), 10 U/ml DNAse I (Worthington, Cat# 54E7315); for 35 min at 37°C with constant agitation (Au & Roskams, 2003). Cells were run through a 40 μm cell strainer to remove non-dissociated tissue pieces and then washed with DMEM-F12 medium. Subsequently, cells were purified by the differential cell adhesion method (Nash, Borke, & Anders, 2001), which consists of three steps: (a) Cells were seeded into uncoated T75 flasks (4×10^6 viable

cells/flask, VWR, Cat# 734–2788, Radnor, PA) for 18 hr to remove fibroblasts; (b) the supernatant of the first step was seeded into another uncoated flask for up to 36 hr to remove astrocytes; and finally (c) the supernatant of the second flask was seeded onto poly-L-lysine (Sigma, Cat# P4707)-coated flasks to grow primary OECs. Cells were cultured for up to 2 weeks and medium was changed every 2–3 days. OECs constituted more than 90% of the cells in the culture based on p75 and S100B immunostaining (data not shown). For OECs to be co-cultured with primary astrocytes, the medium was gradually changed to serum-free medium (Klenke & Taylor-Burds, 2012) supplemented with 5 ng/ml HB-EGF (PeproTech, Cat# 100–47, Rocky Hill, NJ), and B27 (Thermo Fisher Scientific, Cat# A3582901) to provide a medium compatible with astrocyte culture, since serum has been shown to induce astrocyte reactivity (Foo et al., 2011).

Primary astrocyte cultures were obtained by magnetic sorting as previously described (Holt, Stoyanof, & Olsen, 2019), with some modifications. Briefly, 10–20 cortices of PN day 2–4 pups were dissociated using the MACS Neural Tissue Dissociation Kit-T (Miltenyi Biotec, Cat# 130–093-231, Auburn, CA) at 37°C (5% CO^2, 30 min). Non-dissociated tissue was removed using a 40 μm cell strainer (Fisher Scientific, Cat# 22–363-547), and the remaining cell solution was centrifuged (300 g, 5 min). Next, a discontinuous density gradient, prepared using 1:1 albumin-ovomucoid solution (10 mg/ml of each) (Worthington, Cat# OI; GeminiBio, Cat# 700–102P, West Sacramento, CA), was used to remove cell debris and inhibit enzyme activity. The cell pellet was resuspended in 80 μl Hank's Balanced Salt Solution (HBSS) (Gibco, Cat# 14025–092) plus 20 μl anti-GLAST (ACSA-1) MicroBeads (Miltenyi Biotec, Cat# 130–095–825, Auburn, CA) for up to 10^7 cells, and incubated for 10 min (4°C). Cells were washed and incubated in 90 μl HBSS plus 10 μl anti-Biotin MicroBeads for another 15 min (4°C) before running through MACS column for positive selection of astrocytes. Cells were cultured for 1 week and then the same procedure was followed with antiProminin-1 MicroBeads (Miltenyi Biotec, Cat# 130–092-564) for the negative selection of radial glia, followed by another positive selection with anti-GLAST antibody the same day, to increase the purity of astrocyte cultures. Sorted cells were cultured in T25 flasks coated with poly-L-lysine, in 5 ml serum-free astrocyte culture medium (ACM, described above). In our hands, astrocytes isolated by this method and cultured in ACM were not reactive when stained with NFκB (not shown). The same method was adjusted to obtain oligodendrocyte cultures using anti-O4-MicroBeads (Miltenyi Biotec, Cat# 130–096-670). The immortalized mouse astrocyte line C8D30 (ATCC, VA) was cultured in DMEM-F12 (Gibco, Cat# 10313–02, 11765–054, Long Island, NY) containing 10% Fetal Bovine Serum (FBS) (Gibco, Cat# 10438–026), plus 0.5% antibiotic-antimycotic (Gibco, Cat# 15240–062) at 37°C in 5%CO2.

2.3 | Immortalized OEmyc790 cell lines

Six immortalized OEC lines (OEmyc790-C7s.D, D6s.AB8, C6s.BG9, D10, and D4), derived from retrovirus-mediated transformation of primary embryonic mouse OE cultures derived from E15 mouse embryos (Calof & Guevara, 1993), were analyzed; two lines, OEmyc790-C7s.D (C7) and OEmyc790-C4 (C4), were used for the studies described below. Cells were plated on cell culture plates (Fisher Scientific, Cat# 130190, Waltham, MA) and cultured in DMEM-F12 as described above. Medium was changed every 3–5 days. When 60%

confluent, a 1:4 dilution of trypsin was used (Gibco, Cat# 15400054) to split the cells into thirds.

2.4 | Primary antibodies and recombinant proteins

The following antibodies were used: CryAB rabbit polyclonal antibody (Millipore, Cat# ABN185, Darmstadt, Germany), 1:1 K for WB, 1:4 K for immunofluorescence (IF); Histone mouse monoclonal antibody (Fisher Scientific, Cat# AHO1432, Waltham, MA, 1:200 for WB); NFκB rabbit polyclonal antibody (C-20, Santa Cruz, Cat# sc-372, Santa Cruz, CA, 1:650 for WB, 1:750 for IF); Sox10 goat polyclonal antibody (N-20, Santa Cruz, Cat# sc-17342, 1:300 for IF); Alix mouse monoclonal antibody (3A9, Cell Signaling, Cat# 2171 T, 1:1 K for WB); GFAP chicken polyclonal antibody (Aves, 1:4 K for IF); Flotillin-1 rabbit polyclonal antibody (D2V7J, Cell Signaling, Cat# 18634, 1:1 K for WB); β-actin mouse monoclonal antibody (AC-74, Millipore, Cat# A2228, 1:1 K for WB); Tomm20 rabbit polyclonal antibody (FL-145, Santa Cruz, Cat# sc-11415, 1:1 K for WB); CD63 biotinylated antibody (Miltenyi Biotec, Cat# 130–108-922, Auburn, CA, 1:15 for IF); BLBP mouse monoclonal antibody (Abcam, Cat# ab131137, 1:2 K for IF) and p75-NGFR rabbit polyclonal antibody (Millipore, Cat# AB1554, 1:5 K). Recombinant chicken Anosmin1 (MyBioSource, Cat# MBS963562-COA, San Diego, CA) was used at 5 nM while recombinant CryAB protein (MyBioSource, Cat# MBS964495) and recombinant myoglobin (MyBioSource, Cat# MBS142891) were used at 50 ng/ml unless stated otherwise.

2.5 | Mass spectrometry

Primary OECs, and immortalized C7 and C4 OEC cell lines, were established by seeding them in T75 flasks at a concentration of 8×10^5 cells/flask in regular growth medium. To concentrate secreted proteins, the cells in each flask were rinsed and media replaced with 10 ml/flask of Earle's Balanced Salt Solution (EBSS) with 5.5 mM D-Glucose (Gibco, Cat# 14155–063); conditioned medium (CM) was collected after 48 hr total of incubation. For the last 2 hr of the 48-hr collection period, either 1 μl/ml LPS (Sigma, Cat# L6529) or 5 nM recombinant chicken Anosmin1 was added. Anosmin-1 is an extracellular protein secreted by astrocytes (Gianola, de Castro, & Rossi, 2009). Hu, Butts, Poopalasundaram, Graham, and Bouloux (2019) show that loss of function of Anosmin-1 results in abnormal OEC maturation and organization in the ONL (Hu et al., 2019). Here we used bacterial endotoxin LPS as a stress signal and recombinant Anosmin-1 as an extracellular signal from astrocytes in an attempt to stimulate the secretion of anti-inflammatory factors from OECs. One sample for each condition (6 in total) was taken for mass spec analysis. CM was then collected, centrifuged to remove debris, and frozen at −80°C. Frozen samples were freezedried using a lyophilizer (Novalyphe-NL150, Savant Instruments, Holbrook, NY). The pellets were reconstituted in water and bicinchoninic acid (BCA) protein assay was performed. 200 μg/60μl protein per group was submitted for mass spectrometry analysis (NINDS Protein Facility, NIH). Each sample was digested with trypsin. Tandem Mass Tag (TMT) labeled samples were mixed together (TMT 126–131). The mixture was separated using hydrophilic interaction liquid chromatography (HILIC) high performance liquid chromatography (HPLC) system. Five HILIC fractions were collected from the mixed sample. One liquid chromatography–tandem mass spectrometry (LC/MS/MS) experiment was performed for each HILIC fraction, using an Orbitrap Fusion Lumos Mass Spectrometer

(Thermo Fisher Scientific, Waltham, MA) coupled to a 3,000 Ultimate high-pressure liquid chromatography instrument (Thermo Fisher Scientific). Proteome Discoverer 2.2 software used for database search and TMT quantification, and data were mapped against the Sprot mouse database. “Primary OEC + LPS-CM” was used as reference to calculate the ratio for LPS treated samples; “Primary OEC + 5nMA1-CM” was used as reference to calculate the ratio for 5nMAnosmin1-treated samples. No normalization was performed. See Data S1 and S2 for obtained values.

2.6 | Immunoblot analysis

As a readout of reactivity, quantitative immunoblot analysis was performed on nuclear fractions of immortalized C8D30 astrocytes treated with 1 μl/ml LPS or vehicle control for 2 hr. For co-culture groups, OECs seeded on porous inserts (0.4 μm Millicell Cell Culture Insert, Millipore, Cat# PICM0RG50) were placed on top of astrocytes for 24 hr and were discarded at the end of the incubation period, so that only astrocytes were collected for subsequent protein analysis. For the CM treated groups, CM from each line was collected (after 24 hr incubation) and then added to astrocytes for 22 hr, followed by a 2-hr LPS treatment. Astrocytes were then collected by scraping and the CNMCS Compartmental Protein Extraction Kit (BioChain Cat# K3013010 Hayward, CA) with protease/phosphatase inhibitors (PI, Cell Signaling, Cat# 5872S, Danvers, MA) was used and the nuclear fractions were isolated for each treatment condition. The fractions were run on BioRad Mini-Protean TGX Stain-Free Gels (Cat#4568084), transferred to PVDF stain-free blot (Trans-Blot Turbo Transfer Pack, Cat#1704156) via the Trans-Blot Turbo transfer system (BioRad), and blocked with 5% dry milk (BioRad, Cat #170–6404) prior to staining with NFκB antibody. Membranes were exposed to Clarity enhanced chemiluminescence (ECL) reagent (Cat. # 170–5061, Bio-Rad) for 5 min and the signal was detected using ChemiDoc MP (Cat. # 170–8280, Bio-Rad). Quantification of band intensities was calculated using Image Lab 5.0 software (Bio-Rad) and normalized by the loading control immunostained for Histone on the same sample and the same blot. For each biological replicate, values were normalized to “astrocytes + LPS” group. Statistical analysis was performed on the normalized value from biological replicates ($N = 3$).

2.7 | Quantitative immunofluorescence

Fluorescent immunostaining for nuclear NFκB and cytoplasmic NFκB was quantified in immortalized C8D30 astrocytes following 2-hr treatment with 1 μg/ml LPS or a cocktail of three cytokines: Il-1α (3 ng/ml, Sigma, Cat# I3901), TNFα (30 ng/ml, Cell Signaling, Cat# 8902SF) and C1q (400 ng/ml, MyBioSource, Cat# MBS143105, San Diego, CA), as follows: After immunofluorescence staining for NFκB, confocal images were taken on a Zeiss LSM 800 Confocal Microscope (Carl Zeiss, Thornwood, NY). A defined area was measured in both nuclear and cytoplasmic compartments for each astrocyte, and the fluorescence intensity was quantified for each area in each cell using Imaris software. The ratio of nuclear to cytoplasmic fluorescence intensity was used as a quantitative readout of astrocyte reactivity. Median values were calculated for each biological replicate ($N = 3$) obtained from multiple images (2–3/well) containing a total of ~100 cells/treatment (Figure 1c, cell numbers in Table S1) or ~50 cells/treatment (Figure 2b, cell numbers in Table S2). Values greater than one indicate that the NFκB value was higher in the nucleus

compared to cytoplasm, and cells were reactive. Statistics (analysis of variance [ANOVA]) were performed and the average median value ±*SD* per treatment plotted.

2.8 | Isolation of exosomes and exosome uptake experiments

For isolation of exosomes, previously established ultracentrifugation method was used with slight modifications (Adolf et al., 2019; Breglio et al., 2020). Briefly, 24 hr prior to exosome collection, cells were washed and medium changed to exosome depleted medium (EDM) containing 10% exosome-depleted FBS (Gibco, Cat# A27208–03). CM was collected, (protease inhibitor [PI] was added immediately for immunoblotting) and samples kept at 4°C until exosome isolation. Exosomes were isolated through three centrifugation steps: (a) CM was spun for 10 min at 2,000g to remove debris; (b) the resulting supernatant was centrifuged for 30 min at 10,000g to pellet micro-vesicles; and (c) this second supernatant was centrifuged for 4 hr at 100,000g (Optima MAX-XP ultracentrifuge, TLA-100.3 rotor, Beckman Coulter). Following ultracentrifugation, pelleted exosomes were re-suspended in buffer (for ELISA and immunoblotting) or cell culture medium, as required. For astrocyte uptake experiments, isolated OEC-exosomes were resuspended by pipetting and added directly to the culture medium of *CryAB*$^{-/-}$ astrocytes for 4 hr. Cultures were then fixed with 4% paraformaldehyde and stained for markers of interest. Images were taken on a stimulated emission depletion (STED) confocal microscope (Leica, Wetzlar, Germany) for the visualization of internalized exosomes in astrocytes.

2.9 | CryAB immunoprecipitation

CryAB was immunoprecipitated (IP-CryAB) from isolated OEC-exosome fractions that were lysed in RIPA buffer. Briefly, 200 μl Protein A Dynabeads (30 mg/ml, Invitrogen, Cat# 10001D, Carlsbad, CA) were washed three times in PBS+ 0.1% Tween (PBST) using a magnetic stand (Millipore, PureProteome Cat# LSKMAGS08), CryAB antibody (400 μl, 1:50 [10 μg/ml] in PBST) was added to the beads, and the mixture was incubated (30 min, RT) with constant agitation. The antibody solution was removed, beads washed (three times), exosome fractions resuspended in PBS were added, and the mixture was incubated overnight (4°C). Beads were then washed (four times) and CryAB protein eluted by addition of 60 μl of 0.2 M Glycine (pH 2.5); the pH of the eluate was neutralized by addition of 5 μl of 1 M Tris (pH 8.5). Cell culture, immunoblotting or ELISA was performed.

2.10 | ELISA

CryAB concentration was measured in exosome fractions using a competitive ELISA kit (MyBioSource, Cat# MBS7239470, San Diego, CA) according to manufacturer's instructions. Isolated exosomes were sonicated and lysed in Buffer M (containing NP40) plus PI from Protein Extraction Kit (BioChain). Equivalent quantities of total exosomal protein or supernatant CM protein, determined by BCA protein assay, were brought to equivalent volumes in EDM. Then, 100 μl of samples were added to each well and measured with a microplate reader (FlexStation 3; Molecular Devices, Sunnyvale, CA). Results were analyzed with SoftMax Pro Software (Molecular Devices).

2.11 | Quantitative RT-PCR (q-RT-PCR)

cDNA synthesis was performed using Superscript™ III reverse transcriptase (Invitrogen), and PCR carried out using the ViiA7 Real-Time PCR System (Applied Biosystems, Waltham, MA) in 20 μl final volume, containing 10 μl of SsoAdvanced Universal SYBR Green Supermix (BioRad Cat#1725271), 2 μl of a primer mix with a concentration of 1 μM of each primer and 1 μl of cDNA and 7 μl water. Samples were run in triplicate. The expression levels of genes of interest were normalized using the primers (forward; reverse) (AGTGCCAGCCTCGTCCCGTA; TGAGCCCTTCCACAATGCCA), for expression of GAPDH (see Data S3 for obtained values). All other primer sequences are detailed in (Clarke et al., 2018; Liddelow et al., 2017). Data were analyzed by one-way ANOVA followed by Dunnett's multiple post hoc test.

2.12 | Colocalization analysis

Imaging was done via STED confocal microscope for the visualization of internalized exosomes in astrocytes. A single plane and the same parameters (gain, pin size, etc.) were used for all groups. To calculate the covariance of two fluorescent signals, Pearson's colocalization coefficient was used. For quantification, thresholds were determined automatically using Imaris 9.1.0; based on the maximum threshold of intensity for each channel (i.e., above nonspecific staining) that showed any statistical correlation (Costes et al., 2004).

2.13 | Statistical analysis and cell counting

All statistical analyses were done using GraphPad Prism 8.00 software. The results are shown as mean ± *SD*. Statistical analysis was performed using one-way or two-way ANOVA followed by Dunnett's multiple post hoc test, unless otherwise stated. Probability values of .05 ($p \leq .05$) were considered to indicate statistical significance. N = biological replicates, n = technical replicates.

3 | RESULTS

3.1 | OECs secrete anti-inflammatory factor(s) that reduce astrocyte reactivity

Nuclear translocation of the pro-inflammatory protein NFκB was used as a readout of astrocyte reactivity evoked by bacterial endotoxin LPS (Rothhammer et al., 2016), as measured by immunoblot analysis of the nuclear fraction of astrocyte lysates (Figure 1A). As expected, NFκB increased in the nuclear fraction of immortalized C8D30 astrocytes treated with LPS (Figure 1A, gray bars, $p \leq .05$). Co-culture of astrocytes with OECs blocked nuclear translocation of NFκB in response to LPS, as previously reported (Hale et al., 2011; Figure 1A, purple bars). Adding CM from untreated OEC monocultures, (OEC-CM), also decreased NFκB translocation into nuclei of astrocytes exposed to LPS (Figure 1A, red bars), indicating that anti-inflammatory factor(s) are secreted by OECs even in the absence of a stress signal.

To facilitate identification of OEC factors of interest, the anti-inflammatory capacity of six immortalized OEC lines (Calof & Guevara, 1993) were screened. Immortalized astrocytes (C8D30) were treated with CM from the different OEC lines, treated with

LPS, immunostained for NFκB (Figure 1B), and the nuclear/cytoplasmic ratio of NFκB immunostaining was determined. As shown in Figure 1C, CM from two of the immortalized OEC lines, C7, and D6, significantly reduced nuclear NFκB translocation in C8D30 astrocytes compared to LPS treatment alone (Figure 1C, red bars, $p \leq .05$), while D4 and C4 CM were similar to LPS alone. Original characterization of these immortalized OEC lines had been based on morphology and immunostaining with markers expressed by primary OECs (Calof & Guevara, 1993). Characterization of the re-grown lines was consistent with earlier reports, with C7 cells, for example, showing heterogeneous morphologies depending on culture conditions and density (Figure 1D): these included Schwann Cell spindle-like (majority; Figure 1Da), astrocyte-like type1 (Figure 1Db), and astrocyte-like type2 (Figure 1Dc) morphologies (Huang et al., 2008). Cell lines were re-examined by immunofluorescence for expression of OEC-specific markers, such as p75, Sox10, and brain lipid-binding protein (BLBP). Both C7 and C4 cell lines were positive for these OEC markers (Figure 1E and Figure S2). Since C7-CM significantly suppressed nuclear NFκB translocation in astrocytes, whereas C4-CM did not (Figure 1B,C), and both lines expressed the OEC markers tested, C7-CM was used as a positive control, and C4-CM as a negative control in further experiments.

3.2 | OEC-secreted CryAB suppresses LPS-induced astrocyte reactivity

To identify OEC-derived molecules potentially involved in crosstalk between OECs and astrocytes, secreted proteins from primary OEC-CM, C7-CM, and C4-CM were compared by mass spectrometry. Before collection of CM, LPS was added to cultures as a stress signal. Secreted proteins from LPS-treated cells were ranked based on (a) their abundance in C7-CM compared with C4-CM; (b) their abundance in C7-CM compared to primary OEC-CM; and (c) absence from C4-CM (Figure 2a). Proteins that were secreted at similar levels by C7 cells and primary OECs (Figure 2a, horizontal dashed line), but are not likely to be present in C4-CM (Figure 2a, X-axis) were determined. Based on these criteria, we identified two proteins of particular interest: the heat shock protein alpha crystallin B chain (CryAB), and the cell surface glycoprotein MUC18 (MCAM). To identify OEC secreted molecules in response to an endogenous signal from astrocytes, similar experiments were performed after treatment with Anosmin1, an extracellular binding protein secreted by mature astrocytes (Gianola et al., 2009) and shown to act on OECs (Hu et al., 2019). Even though the ortholog is yet to be identified for this protein in mice, we observed a robust migration of primary mouse OECs towards recombinant Anosmin-1 (personal observation). Notably, both CryAB and MCAM were identified as major secreted proteins in this screen as well (Figure 2b). CryAB was selected for further study because of its known role as an anti-inflammatory protein involved in stress responses by CNS glia (e.g., Kuipers et al., 2017; Ousman et al., 2007), and because it was the most abundant protein fitting our criteria in screens of both LPS (Figure 2a) and Anosmin-1 (Figure 2b) treated samples. Recombinant CryAB protein mimicked the effect of OEC-CM or C7-CM on astrocyte reactivity, as measured by suppressed nuclear translocation of NFκB, following either LPS- or cytokine-induced inflammation (Figure 2c). Exosome associated protein myoglobin was used as control.

3.3 | Exosomes secreted by OECs contain CryAB, which moderates intercellular immune response

Since it has been shown that CryAB secretion can occur via exosomes (Guo et al., 2019; Kore & Abraham, 2014; Sreekumar et al., 2010), exosomes were isolated from OECs to determine whether they were positive for CryAB and whether the CryAB secreted via OEC-exosomes had the ability to attenuate astrocyte reactivity. For these experiments, exosome fractions were isolated from culture supernatants of OECs generated from both *CryAB*$^{-/-}$ mice and WT (*CryAB*$^{+/+}$) controls. To ensure the quality of fractions used, exosomes and whole cell lysates (CL) from WT OECs were analyzed by immunoblotting for the following proteins: the structural protein, β-actin; a mitochondrial protein, Tomm20; a nuclear protein, histone H3; and the extravesicular protein Flotilin-1. The exosome fraction was devoid of β-actin, Tomm20, and histone H3, but was positive for Flotilin-1 (Figure 3a), consistent with published information for exosome fractions (Jeppesen et al., 2019). Competitive ELISA against CryAB confirmed the presence of CryAB in OEC exosomes. Exosomes derived from 1×10^6 OECs contained 9.22 ± 0.2 ng CryAB, whereas CryAB protein was undetectable in CM from which exosomes were depleted (Figure S1A). Next, exosomes from both genotypes were immunoblotted for CryAB and the endocytosis protein, Alix, which is concentrated in exosomes (Figure 3b; Jeppesen et al., 2019). CryAB was present in WT OECexo fractions but was absent in *CryAB*$^{-/-}$OECexo fractions; while the exosome marker Alix was present in exosome fractions from OECs of both genotypes. Finally, to assay whether CryAB present in OEC exosomes could suppress astrocyte reactivity, the exosomes were added to immortalized C8D30 astrocytes for 24 hr, and treated with LPS for the last 2 hr of this incubation. As shown in Figure 3c, quantitative immunoblotting demonstrated that: (a) exosomes from WT OECs were able to suppress astrocyte reactivity, as measured by reduced nuclear translocation of NFκB; (b) astrocytes treated with *CryAB*$^{-/-}$OECexo remained reactive; and (c) the reactivity of astrocytes treated with *CryAB*$^{-/-}$OECexo was reduced by the presence of recombinant CryAB protein. Immunostaining OEC-astrocyte co-cultures for NFκB further showed strong nuclear NFκB immunostaining exhibited by astrocytes co-cultured with *CryAB*$^{-/-}$OECs (Figure 3d, lower right). Whereas astrocytes co-cultured with WT OECs showed little if any nuclear NFκB immunostaining (Figure 3d, lower left). Together, these results are consistent with CryAB, secreted by OECs in exosomes being an important protein for OEC-astrocyte crosstalk, and functioning as an anti-inflammatory molecule for astrocytes.

3.4 | Astrocytes internalize CryAB-containing OEC exosomes

To determine whether astrocytes take up CryAB-containing exosomes secreted by OECs, *CryAB*$^{-/-}$ astrocytes were cultured with exosome fractions from OEC cultures generated from WT mice. Uptake was visualized by immunostaining of GFAP-positive astrocytes (Figure 4, magenta); colabeled with antibodies to endosome/ exosome marker CD63 (red) and CryAB (green). CryAB and CD63 colocalized in *CryAB*$^{-/-}$ astrocytes treated with exosomes for 4 hr (Figure 4, insets). Neither untreated *CryAB*$^{-/-}$ astrocytes (Figure 4b) nor WT astrocytes (Figure 4c) showed such specific colocalization (Supplementary Figure 3), consistent with the uptake of CryAB-containing OEC exosomes by astrocytes.

3.5 | OEC secreted factors, including CryAB, reduce astrocytes' expression of genes associated with neurotoxic reactivity

To evaluate the effects of OEC-secreted CryAB on expression of "neurotoxic" genes, astrocytes were exposed to LPS alone; or WT OEC-CM, *CryAB*$^{-/-}$OEC-CM, or CryAB immunoprecipitated from isolated OEC-exosome fractions (IP-CryAB) together with LPS. mRNA from treated astrocytes was then analyzed for 12 transcripts known to be associated with neurotoxic astrocyte reactivity (Liddelow et al., 2017). Q-RT-PCR analysis (Figure 5) showed that all tested transcripts were reduced in expression in the presence of WT OEC-CM, and this effect was significant for 9 of the 12 (Figure 5B, white arrows, $p \leq .05$ A vs. B). In contrast, four of the transcripts showed increased expression when treated with *CryAB*$^{-/-}$OEC-CM (Figure 5C, black arrows). The analysis also suggests that suppression of expression of *Ggta1*, *Serping1*, *Iigp1*, *Gbp2*, and *Amigo2* was CryAB-dependent, for the following reasons: (a) suppression of expression failed to occur with *CryAB*$^{-/-}$OEC-CM treatment, while still taking place with IP-CryAB treatment (Figure 5, C vs. D); or (b) expression was upregulated in the *CryAB*$^{-/-}$OEC-CM group (Figure 5, C vs. A). Suppression of expression of four genes (*H2-T23*, *Srgn*, *H2D1*, and *C3*) appeared to be independent of CryAB, since it still occurred in astrocytes treated with *CryAB*$^{-/-}$OEC-CM (Figure 5, C vs. A). In contrast to either OEC-CM treatments (*CryAB*$^{-/-}$or WT), a significant increase in *Fbln5* was detected in astrocytes treated with IP-CryAB (Figure 5, D vs. A). These results are consistent with the finding that CryAB, secreted by OECs, functions as an anti-inflammatory agent for astrocytes. In addition, comparison of OEC-CM treatment to IP-CryAB for transcripts *Ugt1a1*, *C3*, and *Fbln5* suggest that there are factors in OEC-CM, in addition to CryAB, that suppress neurotoxic astrocyte reactivity.

4 | DISCUSSION

4.1 | OEC-secreted factors that moderate astrocyte reactivity

Astrocyte reactivity is a pathological response that occurs in a wide range of CNS injuries, inflammation and diseases. in vivo studies show that some reactive astrocytes induced by ischemia can promote neural recovery and repair (reviewed in Rossi, Brady, & Mohr, 2007); in contrast, reactive astrocytes induced by bacterial endotoxins such as LPS are neurotoxic (Zamanian et al., 2012). This harmful, neurotoxic astrocyte reactivity appears to be driven by pro-inflammatory cytokines secreted by activated microglia and has been observed in multiple human neurological diseases via C3 staining (Liddelow et al., 2017). However, anti-inflammatory factors that suppress neurotoxic astrocyte reactivity are largely unknown.

OECs, ensheathing glia of the olfactory system, have been shown to improve functional recovery following their transplantation to CNS injury sites (reviewed in Roet & Verhaagen, 2014). In addition, it has been suggested that transplanted OECs could form peripheral-type myelin sheaths around axons (Franklin, Gilson, Franceschini, & Barnett, 1996), and reduce the lesion size in diverse demyelinating environments (Sasaki, Lankford, Radtke, Honmou, & Kocsis, 2011). The selection of OECs for such experiments was based on their repair promoting role in the olfactory system, which is one of the few niches in the mammalian CNS that supports neuronal regeneration throughout life (Forni, Bharti, Flannery, Shimogori, & Wray, 2013). Olfactory sensory neurons are vulnerable to

inflammation and damage due to their exposed location in the nasal cavity yet have a remarkable capacity for regeneration (Calof, Hagiwara, Holcomb, Mumm, & Shou, 1996; Forni et al., 2013), suggesting the presence of robust anti-inflammatory factors in this system. OECs are present along the entire route traversed by the olfactory sensory axons, that is, from the nasal cavity to the olfactory nerve layer in the olfactory bulb, where they can encounter CNS astrocytes (Li et al., 2005; Raisman & Li, 2007; Williams, Franklin, & Barnett, 2004). Communication between OECs and astrocytes in the OB can be regulated by both gap-junctions and via transmission of extracellular factors (Beiersdorfer et al., 2020). Notably, both transplanted OECs (Lakatos et al., 2003; reviewed in Roet & Verhaagen, 2014) and co-cultured OECs (Hale et al., 2011; Lakatos, Franklin, & Barnett, 2000) have been shown to intermingle with astrocytes and to moderate astrocyte activation.

The studies in this report investigate anti-inflammatory factors secreted by OECs that moderate astrocyte reactivity. Administration of these factors may support functional recovery following CNS injury. Mass spectrometry was used to analyze proteins in CM from primary OECs and compared with the CM of immortalized OEC lines with different anti-inflammatory capacities. Two proteins were identified as potential factors that could suppress neurotoxic astrocyte reactivity: MCAM and CryAB. MCAM (also called CD146 or MUC18) is a signaling receptor that can be cleaved from the cell membrane, generating a soluble form that is associated with increased cell migration and invasion (Seftalioglu & Karakoc, 2000), and primarily has been studied in endothelial cell angiogenesis and cancer metastasis (reviewed in Dye, Medic, Ziman, & Coombe, 2013). Studies on multiple sclerosis (MS) patients showed no association between MCAM expression and disease activity (Petersen et al., 2019). In contrast, CryAB treatment of MS patients was associated with a therapeutic outcome, and downregulation of T cell proliferation and pro-inflammatory cytokine production (Quach et al., 2013; van Noort, Bsibsi, Nacken, Verbeek, & Venneker, 2015). In addition, CryAB has been shown to have neuroprotective and regenerative effects in neuroinflammatory animal model systems (Arac et al., 2011; Ousman et al., 2007; van Noort et al., 2015). Moreover, there is a correlation between glial activation and increased CryAB levels in Alexander, Alzheimer's and Parkinson's diseases, as well as traumatic brain injury and stroke (reviewed in Dulle & Fort, 2016). Thus, we investigated the role of OEC-secreted CryAB in OEC-astrocyte crosstalk.

4.2 | Exosomal release of and mediation of inflammation by CryAB

Our results show that OECs secrete CryAB via exosomes, and that these exosomes produce an intercellular anti-inflammatory effect following their uptake by astrocytes. Exosomes are small vesicles packaged inside multivesicular endosomes (MVE) and released into the extracellular matrix when MVE fuse with the plasma membrane (Jeppesen et al., 2019). Subsequent uptake by a neighboring cell initiates intercellular communication. Notably, released exosomes are functional components of the extracellular matrix that can be induced by stress signals but, in contrast to other vesicles released upon stress, they are associated with cell–cell communication rather than apoptosis (Gupta & Pulliam, 2014; Jeppesen et al., 2019). Consistent with our findings, recent studies suggest that CryAB can be secreted by glia in an autocrine manner (Guo et al., 2019; Kore & Abraham, 2014) and play a protective role (Ousman et al., 2007). Although the downstream effects of CryAB in

astrocytes that we demonstrate have yet to be fully explored, one important role of CryAB may be its interaction with transcription factors, including NFkB, to suppress inflammation by inhibition of their nuclear translocation (Qiu et al., 2016; Shao et al., 2013; Zhang et al., 2015). However, exosome-mediated regulation of the astrocytic immune response by OECs may also be a unique interaction, as membrane composition and protein content of exosomes is cell type (Kalra et al., 2012; Keerthikumar et al., 2016; Kim et al., 2015) and context specific (György et al., 2011; Müller, 2012). The robust anti-inflammatory response induced by OEC-secreted CryAB, shown in the present report, may also be a function of concentration, as our results indicate the concentration of CryAB in OEC exosomes to be higher than that found in astrocyte exosomes. Amount of CryAB in OEC secreted exosomes was ~21% higher than that in astrocyte exosomes (Figure S1A) and exposure to LPS increased OEC secreted CryAB concentration by ~25% (Figure S1B), indicating OECs actively respond to stress by either secreting more exosomes or increasing CryAB concentration in exosomes, or both. In addition, exposure to Anosmin1 increased CryAB concentration by ~77% (Figure S1C), compared with control protein recombinant myoglobin, suggesting OECs can actively respond to extracellular astrocyte signals by increasing CryAB concentrations.

4.3 | CryAB, as well as other factors secreted by OECs, can suppress neurotoxic astrocyte reactivity

Stress causes denaturation of correctly folded proteins that can result in their aggregation and binding to CryAB (Muranova, Sudnitsyna, & Gusev, 2018) and subsequent changes in gene expression (Singh et al., 2019). Our results show that OEC-secreted CryAB suppressed expression of a number of genes associated with neurotoxic astrocyte reactivity and indicate that there are additional factor(s) in OEC-CM that can dampen this harmful reactivity. In fact, C3 expression in IP-CryAB +LPS-treated astrocytes, although not significantly different from that observed in astrocytes treated with LPS alone, was significantly greater than expression in astrocytes treated with either OEC-CM groups (Figure 5). C3 is an important marker for neurotoxic astrocytes, made evident by knockout mice showing reduced activity in microglia and astrocytes, and reduced neuron loss (Shi et al., 2017). Moreover, C3 is found colocalized with astrocyte markers in regions of neurodegeneration in human post-mortem tissue (Liddelow et al., 2017). Therefore, more experiments are required to identify OEC-secreted factor(s) that can suppress C3. In this regard, other proteins identified in our mass spectrometric screen, showing smaller changes, may be worthwhile to evaluate. Certainly, crosstalk mechanisms between OECs and surrounding niche cells, including astrocytes, are highly complicated (Chuah et al., 2011). Previous studies have shown that OEC-secreted heparan sulfate proteoglycans (HSPGs) can moderate astrocyte reactivity as measured by astrocyte-OEC mingling (Higginson et al., 2012). Therefore, OEC-HSPGs could account for these additional factors that were not detected in our screen. In addition to unidentified anti-inflammatory factors, absence or suppression of pro-inflammatory factors might also play a role in OEC-CM's effect on astrocyte reactivity. For example, our mass spectrometry screening showed higher concentration of S100A4 and S100A6 proteins in C4-CM compared to pOEC-CM or C7-CM (Figure 2, Data S1, and S2). S100 proteins are known to modulate neuroinflammation (Donato, 2001), and as such are

also candidate molecules that may contribute to the observed difference in the inflammatory reactivity of astrocytes treated with C4-CM versus pOEC-CM or C7-CM.

Our results suggest that OECs also secrete pro-inflammatory factors as evidenced by increased expression of markers of neurotoxic astrocyte reactivity Ggta1, Serping1, Ligp1, Gbp2, when CryAB$^{-/-}$OEC-CM + LPS was used as compared to LPS alone (Figure 5B). This observation is in agreement with studies showing upregulated expression of pro-inflammatory cytokines in rat (Vincent, Choi-Lundberg, Harris, West, & Chuah, 2007) and human OECs following bacterial infection (Dando et al., 2016). However, we show that the cumulative effect OEC-CM has on astrocyte reactivity is anti-inflammatory (Figure 5A). Therefore, the exacerbated expression of Ggta1, Serping1, Ligp1, Gbp2 in the presence of CryAB$^{-/-}$OEC-CM + LPS may be caused by dysregulation of these factors due to the lack of CryAB. Indeed, studies confirm that CryAB deficient cells significantly upregulate expression of TNF-α, IL-6, IL-1β, and IL-8, while lentivirus mediated overexpression of CryAB suppresses their expression by inhibiting NFκB activity (Xu et al., 2019), or by binding secreted proinflammatory proteins (Rothbard et al., 2011).

Recent studies have transformed our perception of astrocytes from a passive structural support network for neurons, to active effectors in the regulation of synaptic transmission, neural excitability, plasticity and recovery. In this paper, we identify OEC secreted CryAB as an anti-inflammatory factor that can moderate astrocyte reactivity, suppressing both transcription of neurotoxic classified genes and nuclear translocation of pro-inflammatory factor NFκB. Improving our understanding of the crosstalk between astrocytes and OECs may inform strategies to identify other endogenous repair mechanisms that facilitate CNS repair, and consequently impact function, in the injured nervous system.

Supplementary Material

Refer to Web version on PubMed Central for supplementary material.

ACKNOWLEDGMENTS

We thank Dr. S. Kawauchi for help transferring OEmyc790 cell lines; Dr. Y. Li and the NINDS Protein/Peptide Sequencing Facility for mass spectrometry analysis; Dr. L. Dong and the NEI transgenic mouse core for providing cryopreserved sperm from *CryAB*$^{-/-}$ mice; Dr. J. Pickel and the NIMH transgenic mouse core facility for rejuvenation of mice; Dr. V. Schram and the NINDS Light Imaging Facility for use of the confocal scanning and STED microscopy. We also thank the Amara Lab, Sibley Lab, and Friedman Lab for the use equipment. Dr. Y. Shan, Dr. J. Chen, Dr. S. Inagaki, and S. Robertson for technical assistance. We are grateful to Drs E. Quinlan, S. Constantin, H. Cho, N. Whittington, P. Yuen, J. Street, and M. Barzik for providing helpful advice. This work was supported by the Intramural Research Program of the National Institutes of Health, National Institute of Neurological Disorders and Stroke (ZIA NS002824). The authors declare that there are no potential conflicts of interest.

Funding information

National Institute of Neurological Disorders and Stroke; National Institutes of Health

DATA AVAILABILITY STATEMENT

The data that supports the findings of this study are available in the supplementary material of this article.

REFERENCES

Adolf A, Rohrbeck A, Münster-Wandowski A, Johansson M, Kuhn HG, Kopp MA, … Höltje M. (2019). Release of astroglial vimentin by extracellular vesicles: Modulation of binding and internalization of C3 transferase in astrocytes and neurons. Glia, 67(4), 703–717. 10.1002/glia.23566 [PubMed: 30485542]

Arac A, Brownell SE, Rothbard JB, Chen C, Ko RM, Pereira MP, … Steinberg GK (2011). Systemic augmentation of alpha B-crystallin provides therapeutic benefit twelve hours post-stroke onset via immune modulation. Proceedings of the National Academy of Sciences, 108, 13287–13292. 10.1073/pnas.1107368108

Au E, & Roskams AJ (2003). Olfactory ensheathing cells of the lamina propria in vivo and in vitro. Glia, 41(3), 224–236. 10.1002/glia.10160 [PubMed: 12528178]

Beiersdorfer A, Wolburg H, Grawe J, Scheller A, Kirchhoff F, & Lohr C. (2020). Sublamina-specific organization of the blood brain barrier in the mouse olfactory nerve layer. Glia, 68, 631–645. 10.1002/glia.23744 [PubMed: 31696993]

Brady JP, Garland DL, Green DE, Tamm ER, Giblin FJ, & Wawrousek EF (2001). B-Crystallin in lens development and muscle integrity: A gene knockout approach. Investigative Ophthalmology & Visual Science, 42, 2924–2934. [PubMed: 11687538]

Breglio AM, May LA, Barzik M, Welsh NC, Francis SP, Costain TQ, … Cunningham LL (2020). Exosomes mediate sensory hair cell protection in the inner ear. The Journal of Clinical Investigation, 130, 2657–2672. 10.1172/JCI128867 [PubMed: 32027617]

Calof AL, & Guevara JL (1993). Cell lines derived from retrovirus-mediated oncogene transduction into olfactory epithelium cultures. Methods in Neurosciences, 3, 222–231. 10.1006/ncmn.1993.1057

Calof AL, Hagiwara N, Holcomb JD, Mumm JS, & Shou J. (1996). Neurogenesis and cell death in olfactory epithelium. Journal of Neurobiology, 30(1), 67–81. 10.1002/(SICI)1097-4695(199605)30:1<67::AID-NEU7>3.0.CO;2-E [PubMed: 8727984]

Chuah MI, Hale DM, & West AK (2011). Interaction of olfactory ensheathing cells with other cell types in vitro and after transplantation: Glial scars and inflammation. Experimental Neurology, 229, 46–53. 10.1016/j.expneurol.2010.08.012 [PubMed: 20713050]

Clarke LE, Liddelow SA, Chakraborty C, Münch AE, Heiman M, & Barres BA (2018). Normal aging induces A1-like astrocyte reactivity. Proceedings of the National Academy of Sciences of the United States of America, 115(8), E1896–E1905. 10.1073/pnas.1800165115 [PubMed: 29437957]

Costes SV, Daelemans D, Cho EH, Dobbin Z, Pavlakis G, & Lockett S. (2004). Automatic and quantitative measurement of protein-protein colocalization in live cells. Biophysical, 86(6), 3993–4003. 10.1529/biophysj.103.038422.

D'Agostino M, Lemma V, Chesi G, Stornaiuolo M, Serio MC, D'Ambrosio C, … Bonatti S. (2013). The cytosolic chaperone α-crystallin B rescues folding and compartmentalization of misfolded multispan transmembrane proteins. Journal of Cell Science, 126(18), 4160–4172. 10.1242/jcs.125443 [PubMed: 23843626]

Dairaghi L, Flannery E, Giacobini P, Saglam A, Saadi H, Constantin S, … Wray S. (2018). Reelin can modulate migration of olfactory ensheathing cells and gonadotropin releasing hormone neurons via the canonical pathway. Frontiers in Cellular Neuroscience, 12, 228–241. 10.3389/fncel.2018.00228 [PubMed: 30127721]

Dando SJ, Ipe DS, Batzloff M, Sullivan MJ, Crossman DK, Crowley M, … Ulett GC (2016). Burkholderia pseudomallei capsule exacerbates respiratory melioidosis but does not afford protection against antimicrobial signaling or bacterial killing in human olfactory ensheathing cells. Infection and Immunity, 84(7), 1941–1956. 10.1128/IAI.01546-15 . [PubMed: 27091931]

Donato R. (2001). S100: A multigenic family of calcium-modulated proteins of the EF-hand type with intracellular and extracellular functional roles. The International Journal of Biochemistry & Cell Biology, 33). Retrieved from, 637–668. www.elsevier.com/locate/ijbcb

Dulle JE, & Fort PE (2016). Crystallins and neuroinflammation: The glial side of the story. Biochimica et Biophysica Acta - General Subjects, 1860(1), 278–286. 10.1016/j.bbagen.2015.05.023

Dye DE, Medic S, Ziman M, & Coombe DR (2013). Melanoma biomolecules: Independently identified but functionally intertwined. Frontiers in Oncology, 3, 1–17. 10.3389/fonc.2013.00252 [PubMed: 23373009]

Foo LC, Allen NJ, Bushong EA, Ventura PB, Chung WS, Zhou L, … Barres BA (2011). Development of a method for the purification and culture of rodent astrocytes. Neuron, 71, 799–811. 10.1016/j.neuron.2011.07.022 [PubMed: 21903074]

Forni PE, Bharti K, Flannery EM, Shimogori T, & Wray S. (2013). The indirect role of fibroblast growth factor-8 in defining neurogenic niches of the olfactory/GnRH systems. Journal of Neuroscience, 33(50), 19620–19634. 10.1523/JNeurosci.3238-13.2013

Franklin RJM, Gilson JM, Franceschini IA, & Barnett SC (1996). Schwann cell-like myelination following transplantation of an olfactory bulb-ensheathing cell line into areas of demyelination in the adult CNS. Glia, 17, 217–224. 10.1002/(SICI)1098-1136(199607)17:3<217::AID-GLIA4>3.0.CO;2-Y [PubMed: 8840163]

Gianola S, de Castro F, & Rossi F. (2009). Anosmin-1 stimulates outgrowth and branching of developing Purkinje axons. Neuroscience, 158 (2), 570–584. 10.1016/j.neuroscience.2008.10.022 [PubMed: 19013504]

Giovannoni F, & Quintana FJ (2020). The role of astrocytes in CNS inflammation. Trends in Immunology, 41, 805–819. 10.1016/j.it.2020.07.007 [PubMed: 32800705]

Guo Y. s., Liang PZ, Lu SZ, Chen R, Yin YQ, & Zhou JW (2019). Extracellular αB-crystallin modulates the inflammatory responses. Biochemical and Biophysical Research Communications, 508(1), 282–288. 10.1016/j.bbrc.2018.11.024 [PubMed: 30497777]

Gupta A, & Pulliam L. (2014). Exosomes as mediators of neuroinflammation. Journal of Neuroinflammation, 11, 1–10. 10.1186/1742-2094-11-68 [PubMed: 24383930]

György B, Szabó TG, Pásztói M, Pál Z, Misják P, Aradi B, … Buzás EI (2011). Membrane vesicles, current state-of-the-art: Emerging role of extracellular vesicles. Cellular and Molecular Life Sciences, 68, 2667–2688. 10.1007/s00018-011-0689-3 [PubMed: 21560073]

Hale DM, Ray S, Leung JY, Holloway AF, Chung RS, West AK, & Chuah MI (2011). Olfactory ensheathing cells moderate nuclear factor kappaB translocation in astrocytes. Molecular and Cellular Neurosciences, 46, 213–221. 10.1016/j.mcn.2010.09.004 [PubMed: 20840869]

Higginson JR, Thompson SM, Santos-Silva A, Guimond SE, Turnbull JE, & Barnett SC (2012). Differential Sulfation remodelling of Heparan Sulfate by extracellular 6-O-sulfatases regulates fibroblast growth factor-induced boundary formation by glial cells: Implications for glial cell transplantation. The Journal of Neuroscience, 32, 15902–15912. 10.1523/JNeurosci.6340-11.2012 [PubMed: 23136428]

Holt LM, Stoyanof ST, & Olsen ML (2019). Magnetic cell sorting for in vivo and in vitro astrocyte, neuron, and microglia analysis. Current Protocols in Neuroscience, 88, e71. 10.1002/cpns.71 [PubMed: 31216394]

Hu Y, Butts T, Poopalasundaram S, Graham A, & Bouloux PM (2019). Extracellular matrix protein anosmin-1 modulates olfactory ensheathing cell maturation in chick olfactory bulb development. European Journal of Neuroscience, 50(9), 3472–3486. 10.1111/ejn.14483 [PubMed: 31199027]

Huang ZH, Wang Y, Cao L, Da Su Z, Zhu YL, Chen YZ, … He C. (2008). Migratory properties of cultured olfactory ensheathing cells by single-cell migration assay. Cell Research, 18, 479–490. 10.1038/cr.2008.38 [PubMed: 18347613]

Imaizumi T, Lankford KL, Burton WV, Fodor WL, & Kocsis JD (2000). Xenotransplantation of transgenic pig olfactory ensheathing cells promotes axonal regeneration in rat spinal cord. Nature Biotechnology, 18, 949–953. 10.1038/79432

Jeppesen DK, Fenix AM, Franklin JL, Higginbotham JN, Zhang Q, Zimmerman LJ, … Coffey RJ (2019). Reassessment of exosome composition. Cell, 177(2), 428–445.e18. 10.1016/j.cell.2019.02.029 [PubMed: 30951670]

Johansson S, Lee IH, Olson L, & Spenger C. (2005). Olfactory ensheathing glial co-grafts improve functional recovery in rats with 6-OHDA lesions. Brain, 128, 2961–2976. 10.1093/brain/awh644 [PubMed: 16251218]

Kalra H, Simpson RJ, Ji H, Aikawa E, Altevogt P, Askenase P, … Mathivanan S. (2012). Vesiclepedia: A compendium for extracellular vesicles with continuous community annotation. PLoS Biology, 10, e1001450. 10.1371/journal.pbio.1001450

Keerthikumar S, Chisanga D, Ariyaratne D, Al Saffar H, Anand S, Zhao K, … Mathivanan S. (2016). ExoCarta: A web-based compendium of Exosomal cargo. Journal of Molecular Biology, 428, 688–692. 10.1016/j.jmb.2015.09.019 [PubMed: 26434508]

Kim DK, Lee J, Kim SR, Choi DS, Yoon YJ, Kim JH, … Gho YS (2015). EVpedia: A community web portal for extracellular vesicles research. Bioinformatics, 31, 933–939. 10.1093/bioinformatics/btu741 [PubMed: 25388151]

Klenke U, & Taylor-Burds C. (2012). Culturing embryonic nasal explants for developmental and physiological study. Current Protocols in Neuroscience, 59, 1–22. 10.1002/0471142301.ns0325s59

Kore RA, & Abraham EC (2014). Inflammatory cytokines, interleukin-1 beta and tumor necrosis factor-alpha, upregulated in glioblastoma multiforme, raise the levels of CRYAB in exosomes secreted by U373 glioma cells. Biochemical and Biophysical Research Communications, 453, 326–331. 10.1016/j.bbrc.2014.09.068 [PubMed: 25261722]

Kuipers HF, Yoon J, Van Horssen J, Han MH, Bollyky PL, Palmer TD, & Steinman L. (2017). Phosphorylation of αB-crystallin supports reactive astrogliosis in demyelination. Proceedings of the National Academy of Sciences of the United States of America, 114(9), E1745–E1754. 10.1073/pnas.1621314114 [PubMed: 28196893]

Lakatos A, Barnett SC, & Franklin RJM (2003). Olfactory ensheathing cells induce less host astrocyte response and chondroitin sulphate proteoglycan expression than Schwann cells following transplantation into adult CNS white matter. Experimental Neurology, 184, 237–246. 10.1016/S0014-4886(03)00270-X [PubMed: 14637095]

Lakatos A, Franklin RJM, & Barnett SC (2000). Olfactory ensheathing cells and Schwann cells differ in their in vitro interactions with astrocytes. Glia, 32, 214–225. 10.1002/1098-1136(200012)32:3<214::AID-GLIA20>3.0.CO;2-7 [PubMed: 11102963]

Li Y, Field PM, & Raisman G. (1997). Repair of adult rat corticospinal tract by transplants of olfactory ensheathing cells. Science, 277(5334), 2000–2002. 10.1126/science.277.5334.2000 [PubMed: 9302296]

Li Y, Field PM, & Raisman G. (2005). Olfactory ensheathing cells and olfactory nerve fibroblasts maintain continuous open channels for regrowth of olfactory nerve fibres. Glia, 52(3), 245–251. 10.1002/glia.20241 [PubMed: 15968636]

Liddelow SA, & Barres BA (2017). Reactive astrocytes: Production, function, and therapeutic potential. Immunity, 46(6), 957–967. 10.1016/j.immuni.2017.06.006 [PubMed: 28636962]

Liddelow SA, Guttenplan KA, Clarke LE, Bennett FC, Bohlen CJ, Schirmer L, … Barres BA (2017). Neurotoxic reactive astrocytes are induced by activated microglia. Nature, 541(7638), 481–487. 10.1038/nature21029 [PubMed: 28099414]

Liu T, Zhang L, Joo D, & Sun SC (2017). NF-κB signaling in inflammation. Signal Transduction and Targeted Therapy, 2, 1–9. 10.1038/sigtrans.2017.23

Müller G. (2012). Microvesicles/exosomes as potential novel biomarkers of metabolic diseases. Diabetes, Metabolic Syndrome and Obesity: Targets and Therapy, 5, 247–282. 10.2147/dmso.s32923 [PubMed: 22924003]

Muranova LK, Sudnitsyna MV, & Gusev NB (2018). αB-Crystallin phosphorylation: Advances and problems. Biochemistry (Moscow), 83, 1196–1206. 10.1134/S000629791810005X [PubMed: 30472957]

Nash HH, Borke RC, & Anders JJ (2001). New method of purification for establishing primary cultures of Ensheathing cells from the adult olfactory bulb. Glia, 34, 81–87. 10.1002/glia.1043 [PubMed: 11307157]

O'Toole DA, West AK, & Chuah MI (2007). Effect of olfactory ensheathing cells on reactive astrocytes in vitro. Cellular and Molecular Life Sciences, 64, 1303–1309. 10.1007/s00018-0077-106-y [PubMed: 17447004]

Ousman SS, Tomooka BH, Van Noort JM, Wawrousek EF, O'Conner K, Hafler DA, … Steinman L. (2007). Protective and therapeutic role for αB-crystallin in autoimmune demyelination. Nature, 448, 474–479. 10.1038/nature05935 [PubMed: 17568699]

Petersen ER, Ammitzbøll C, Søndergaard HB, Oturai AB, Sørensen PS, Nilsson AC, … Sellebjerg F. (2019). Expression of melanoma cell adhesion molecule-1 (MCAM-1) in natalizumab-treated multiple sclerosis. Journal of Neuroimmunology, 337, 577085. 10.1016/j.jneuroim.2019.577085

Qiu J, Yan Z, Tao K, Li Y, Li Y, Li J, … Chen H. (2016). Sinomenine activates astrocytic dopamine D2 receptors and alleviates neuroinflammatory injury via the CRYAB/STAT3 pathway after ischemic stroke in mice. Journal of Neuroinflammation, 13(1), 263. 10.1186/s12974-016-0739-8 [PubMed: 27724964]

Quach QL, Metz LM, Thomas JC, Rothbard JB, Steinman L, & Ousman SS (2013). CRYAB modulates the activation of CD4+ T cells from relapsing-remitting multiple sclerosis patients. Multiple Sclerosis Journal, 19(14), 1867–1877. 10.1177/1352458513489853 [PubMed: 23736536]

Raisman G, & Li Y. (2007). Repair of neural pathways by olfactory ensheathing cells. Nature Reviews Neuroscience, 8(April), 313–319. 10.1038/nrn2099

Ramer LM, Au E, Richter MW, Liu J, Tetzlaff W, & Roskams AJ (2004). Peripheral olfactory Ensheathing cells reduce scar and cavity formation and promote regeneration after spinal cord injury. The Journal of Comparative Neurology, 473, 1–15. 10.1002/cne.20049 [PubMed: 15067714]

Roet KCD, & Verhaagen J. (2014). Understanding the neural repair-promoting properties of olfactory ensheathing cells. Experimental Neurology, 261, 594–609. 10.1016/j.expneurol.2014.05.007 [PubMed: 24842489]

Rossi DJ, Brady JD, & Mohr C. (2007, November). Astrocyte metabolism and signaling during brain ischemia. Nature Neuroscience, 10, 1377–1386. 10.1038/nn2004 [PubMed: 17965658]

Rothbard JB, Kurnellas MP, Brownell S, Adams CM, Su L, Axtell RC, … Steinman L. (2012). Therapeutic effects of systemic administration of chaperone αB-crystallin associated with binding proinflammatory plasma proteins. Journal of Biological Chemistry, 287 (13), 9708–9721. 10.1074/jbc.M111.337691. [PubMed: 22308023]

Rothhammer V, Mascanfroni ID, Bunse L, Takenaka MC, Kenison JE, Mayo L, … Quintana FJ (2016). Type I interferons and microbial metabolites of tryptophan modulate astrocyte activity and central nervous system inflammation via the aryl hydrocarbon receptor. Nature Medicine, 22(6), 586–597. 10.1038/nm.4106

Sasaki M, Lankford KL, Radtke C, Honmou O, & Kocsis JD (2011). Remyelination after olfactory ensheathing cell transplantation into diverse demyelinating environments. Experimental Neurology, 229, 88–98. 10.1016/j.expneurol.2011.01.010 [PubMed: 21281634]

Seftalioglu A, & Karakoc L. (2000). Expression of CD146 adhesion molecules (MUC18 or MCAM) in the thymic microenvironment. Acta Histochemica, 102, 69–83. 10.1078/0065-128100544 [PubMed: 10726166]

Shao W, Zhang SZ, Tang M, Zhang XH, Zhou Z, Yin YQ, … Zhou JW (2013). Suppression of neuroinflammation by astrocytic dopamine D2 receptors via αb-crystallin. Nature, 494(7435), 90–94. 10.1038/nature11748 [PubMed: 23242137]

Shi Q, Chowdhury S, Ma R, Le KX, Hong S, Caldarone BJ, … Lemere CA (2017). Complement C3 deficiency protects against neurodegeneration in aged plaque-rich APP/PS1 mice. Science Translational Medicine, 9, eaaf6295. 10.1126/scitranslmed.aaf6295

Silver J, Schwab ME, & Popovich PG (2015). Central nervous system regenerative failure: Role of oligodendrocytes, astrocytes, and microglia. Cold Spring Harbor Perspectives in Biology, 7(3), 1–22. 10.1101/cshperspect.a020602

Singh JP, Kumar RR, Goswami S, Rai GK, Sakhare A, Kumar S, … Praveen S. (2019). A putative heat-responsive transcription factor (TaHD97) and its targets in wheat (Triticum aestivum) providing thermotolerance. Indian Journal of Biotechnology, 18, 214–223. http://nopr.niscair.res.in/handle/123456789/53098

Sofroniew MV, & Vinters HV (2010). Astrocytes: Biology and pathology. Acta Neuropathologica, 119, 7–35. 10.1007/s00401-009-0619-8 [PubMed: 20012068]

Sreekumar PG, Kannan R, Kitamura M, Spee C, Barron E, Ryan SJ, & Hinton DR (2010). αB crystallin is apically secreted within exosomes by polarized human retinal pigment epithelium and provides neuroprotection to adjacent cells. PLoS One, 5(10), e12578. 10.1371/journal.pone.0012578

van Noort JM, Bsibsi M, Nacken PJ, Verbeek R, & Venneker EHG (2015). Therapeutic intervention in multiple sclerosis with alpha B-crystallin: A randomized controlled phase IIa trial. PLoS One, 10(11), e0143366. 10.1371/journal.pone.0143366

Vincent AJ, Choi-Lundberg DL, Harris JA, West AK, & Chuah MI (2007). Bacteria and PAMPs activate nuclear factor kappaB and Gro production in a subset of olfactory ensheathing cells and astrocytes but not in Schwann cells. Glia, 55(9), 905–916. [PubMed: 17427933]

Williams SK, Franklin RJM, & Barnett SC (2004). Response of olfactory ensheathing cells to the degeneration and regeneration of the peripheral olfactory system and the involvement of the Neuregulins. Journal of Comparative Neurology, 470(1), 50–62. 10.1002/cne.11045 [PubMed: 14755525]

Xu W, Guo Y, Huang Z, Zhao H, Zhou M, Huang Y, … Du P. (2019). Small heat shock protein CRYAB inhibits intestinal mucosal inflammatory responses and protects barrier integrity through suppressing IKKβ activity. Mucosal Immunology, 12, 1291–1303. 10.1038/s41385-019-0198-5 [PubMed: 31481750]

Zamanian JL, Xu L, Foo LC, Nouri N, Zhou L, Giffard RG, & Barres BA (2012). Genomic analysis of reactive Astrogliosis. The Journal of Neuroscience, 32, 6391–6410. 10.1523/JNeurosci.6221-11.2012 [PubMed: 22553043]

Zhang Y, Chen Y, Wu J, Manaenko A, Yang P, Tang J, … Zhang JH (2015). Activation of dopamine D2 receptor suppresses neuroinflammation through αb-crystalline by inhibition of NF-κB nuclear translocation in experimental ICH mice model. Stroke, 46(9), 2637–2646. 10.1161/Strokeaha.115.009792 [PubMed: 26251254]

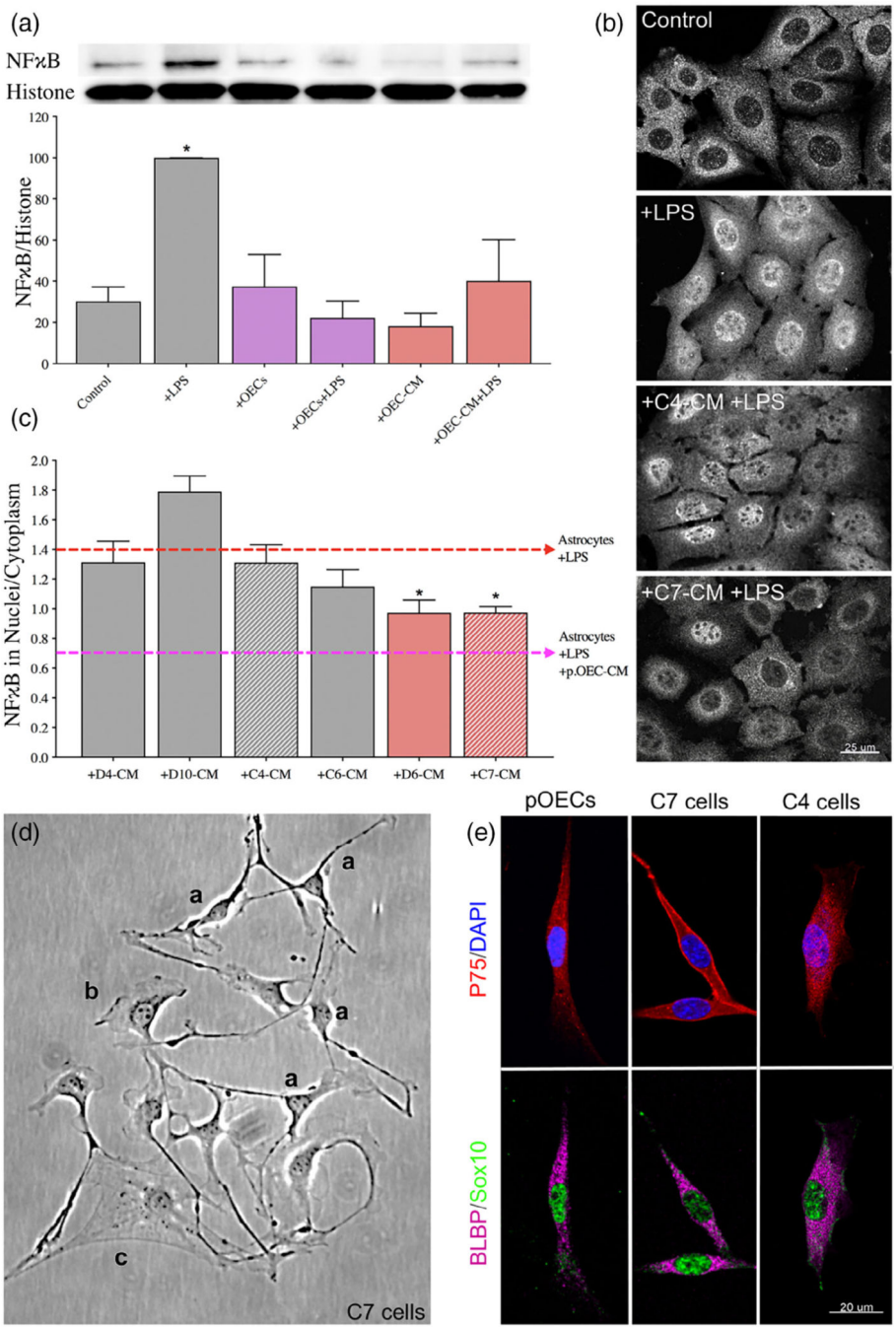

FIGURE 1.

OEC-CM alone is sufficient to suppress LPS-induced astrocyte reactivity, an effect mimicked by a subset of immortalized OEC lines. (A) Quantitative immunoblotting for NFκB was performed on the nuclear fraction of C8D30 astrocyte lysates (inset). All groups were compared using a one-way ANOVA ($N = 3$). Treatment with LPS for 2 hr significantly increased NFκB activity (* indicates $p \leq .05$, gray bars). The presence of OECs blocked the effect of LPS (purple bars). OEC conditioned medium (OEC-CM) alone also blocked the increase in nuclear NFκB (red bars). (B and C) CM from six immortalized OEC lines

were investigated for their ability to block the effect of LPS on nuclear NFκB translocation in C8D30 astrocytes, as measured by the ratio of fluorescence intensity of nuclear to cytoplasmic NFκB. (B) Photomicrograph of images of C8D30 astrocytes cocultured with CM of immortalized cell lines. (C) Fluorescent NFκB nuclear and cytoplasmic intensities were measured and ratios plotted. Pink dashed line depicts value of astrocytes treated with primary OEC-CM + LPS and red dashed line depicts value of astrocytes +LPS. A median value was calculated from ~100 cells per field, and then a mean/group was calculated. C7-CM and D6-CM decreased NFκB nuclear translocation ($N = 3$; $*p \leq .05$; one-way ANOVA), while C4-CM treated groups was not significantly different than astrocytes +LPS alone ($N = 3$; $*p \leq .05$; one-way ANOVA). (D) Photomicrograph from line C7. Multiple morphologies were found in all the OEC cell lines: (a) Schwann Cell-like, (b) astrocyte-like type1, and (c) astrocyte-like type2. Schwann cell-like spindle cells (a) predominated in C7. (E) C7 and C4 olfactory cell lines share multiple markers with OECs including BLBP (magenta), Sox10 (green), and P75 (red). Scale bars represent 25 and 20 μm

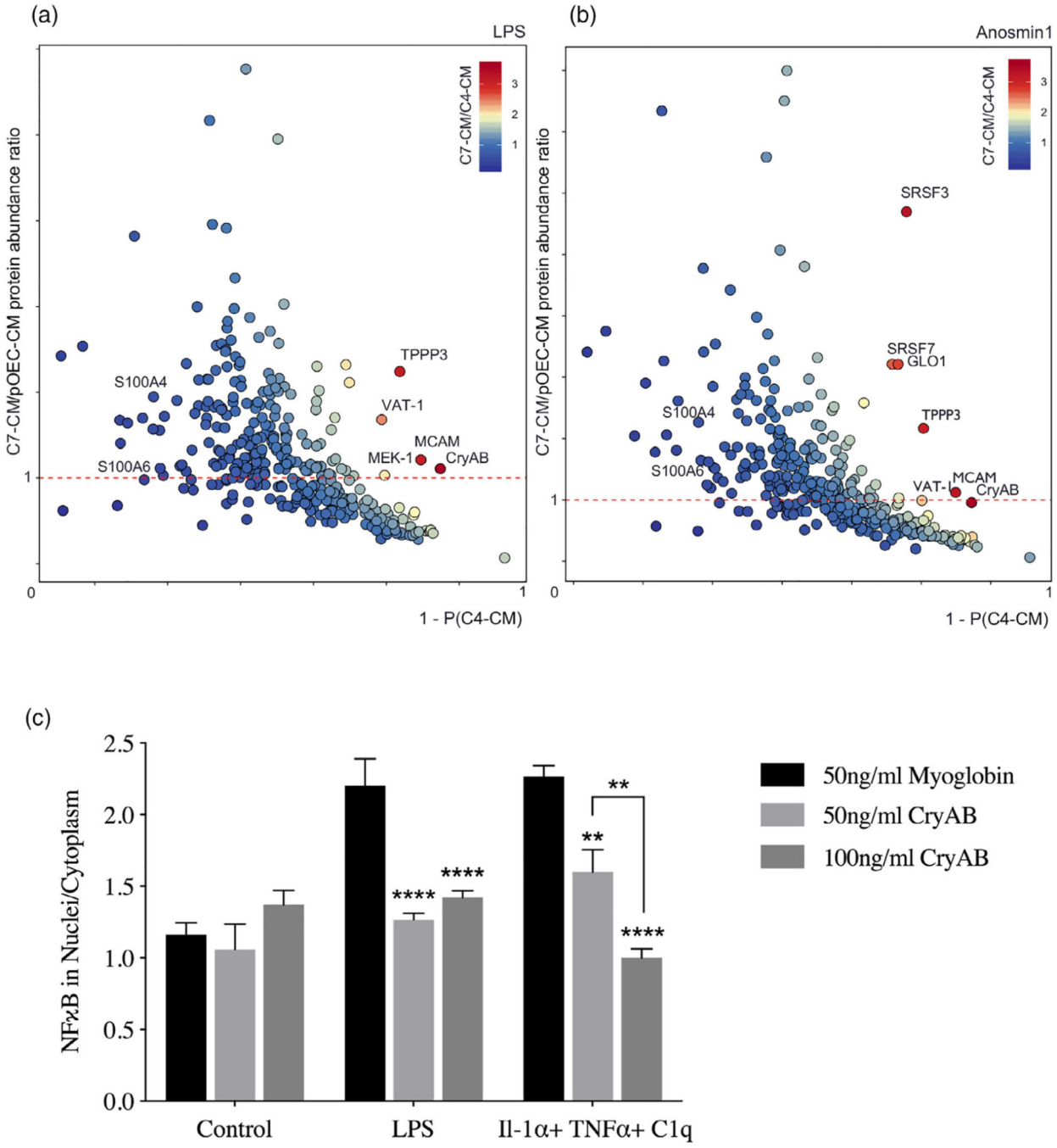

FIGURE 2.

OEC-secreted anti-inflammatory protein CryAB and recombinant CryAB is sufficient to suppress astrocyte reactivity measured by NFκB. (a, b) Comparison of factors secreted from C7 line, C4 line and primary OECs (pOECs), analyzed by mass spectrometry. Proteins detected in CM following LPS treatment (a) or Anosmin1 treatment (b) were ranked by their relative abundance indicated by color code (heat map, inset). Relative abundance of detected proteins in C7-CM compared with pOEC-CM is graphed on the Y-axes, and relative absence of the same proteins from C4-CM (1-P[C4-CM] = probability of not being found in C4-

CM) is graphed on the X axes. Proteins of similar abundance in CMs from C7 cells and pOECs (horizontal red-dashed lines), and not likely to be present in C4-CM (Y-axes) were identified. Alpha crystallin B chain (CryAB) had the highest C7/C4 expression ratio and was equally abundant in CM from C7 cells and pOECs. (c) Recombinant CryAB alone suppressed the inflammatory response, quantified as the ratio of nuclear to cytoplasmic NFκB (Y-axis) in astrocytes exposed to either LPS or a cocktail of the cytokines Il-1α, TNFα, and C1q for 2 hr. Exosome associated protein myoglobin was used as control. Group values were obtained from triplicate wells in which a median value was calculated from ~50 cells per field. $N = 3$; (*$p \leq .05$; **$p \leq .01$; ****$p \leq .0001$;) two-way ANOVA

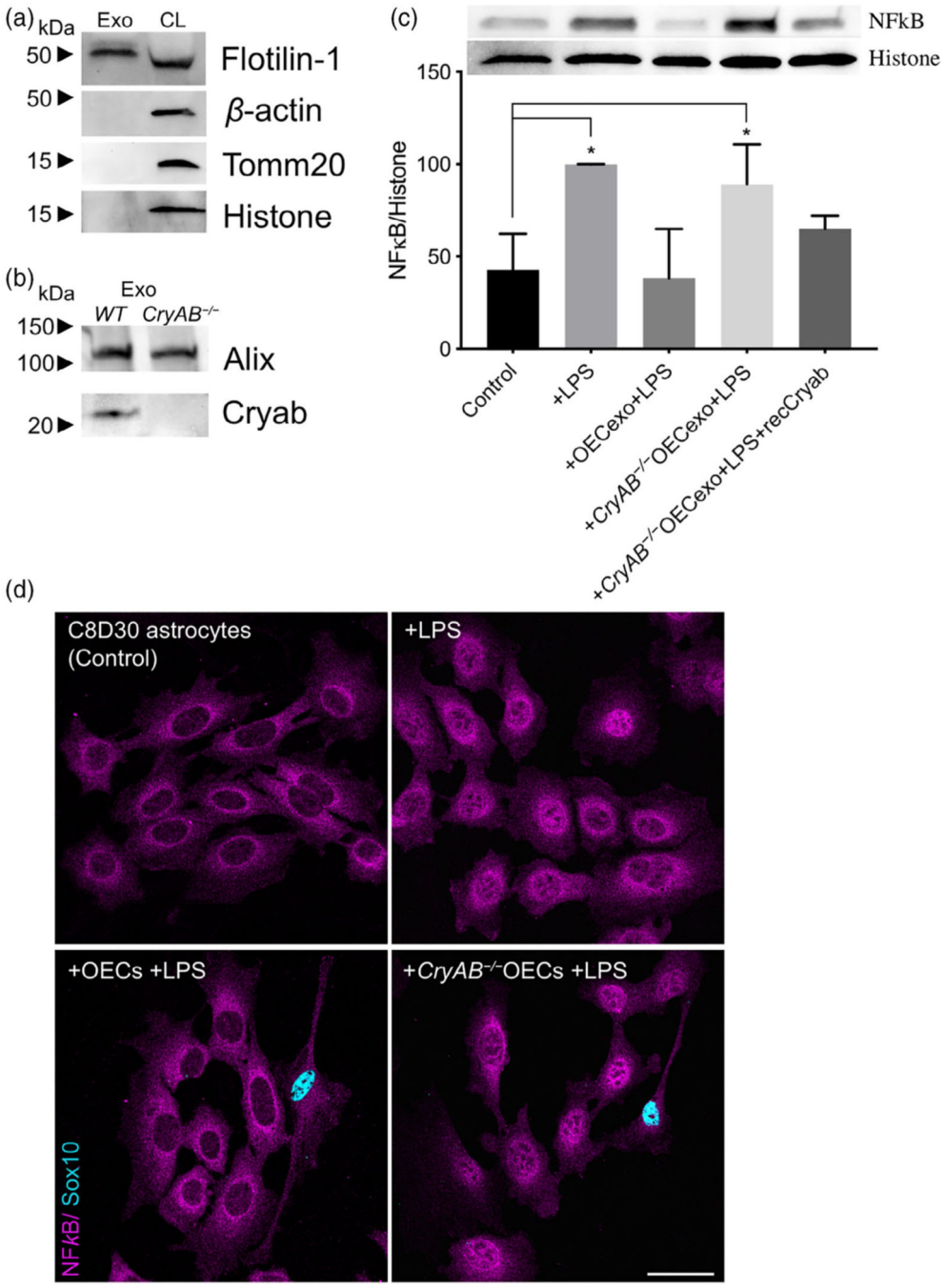

FIGURE 3.

CryAB, secreted by primary OECs into exosomes, suppresses inflammatory response in an astrocyte cell line. (a) Immunoblot of exosome (Exo, left) and whole cell lysate (CL, right) fractions from WT primary OECs were screened for β-actin, Tomm20, histone H3, and Flotilin-1. The exosome fraction from WT exosomes was devoid of cellular β-actin, Tomm20, and histone H3, but contained the extravesicular protein Flotilin-1. (b) Immunoblots for CryAB and the exosome marker Alix were performed on exosome fractions made from *CryAB*$^{-/-}$ and WT (*CryAB*$^{+/+}$) OEC cultures. CryAB was absent in

exosome fractions from *CryAB*$^{-/-}$ OEC culture medium, whereas the exosome marker Alix was present. (c) C8D30 astrocytes were treated for 24 hr with exosomes isolated from WT or *CryAB*$^{-/-}$ OECs. Astrocytes were exposed to 1 μg/ml LPS for the last 2 hr of exosome treatment. Nuclear fractions of astrocytes were analyzed via quantitative immunoblotting for NFκB and Histone H3. Inset shows a representative immunoblot and graph shows mean ± *SD* of NFκB/histone ratio. All conditions were compared with astrocyte alone group (Control, $N = 3$; $p \leq .05$; one-way ANOVA). Treatment of astrocytes with WT OEC-exosomes (exo) + LPS, blocked nuclear NFκB translocation. In contrast, *CryAB*$^{-/-}$OEC-exosomes failed to suppress nuclear NFκB translocation. Recombinant CryAB (50 ng/ml) added to *CryAB*$^{-/-}$OEC-exosomes was sufficient to attenuate NFκB translocation induced by LPS, with levels comparable to WT OEC-exo + LPS. (d) C8D30 astrocytes treated with LPS for 2 hr (top right: "+ LPS") showed stronger immunostaining for NFκB in the nucleus (magenta) compared to untreated controls (top left). Astrocytes co-cultured with *CryAB*$^{-/-}$ OECs (Sox 10-positive cells with blue nuclei) had increased levels of NFκB immunostaining in the nucleus (bottom right: "+*CryAB*$^{-/-}$OECs +LPS") compared with astrocytes co-cultured with WT OECs (bottom left: "+OECs +LPS"). Scale bar represents 40 μm

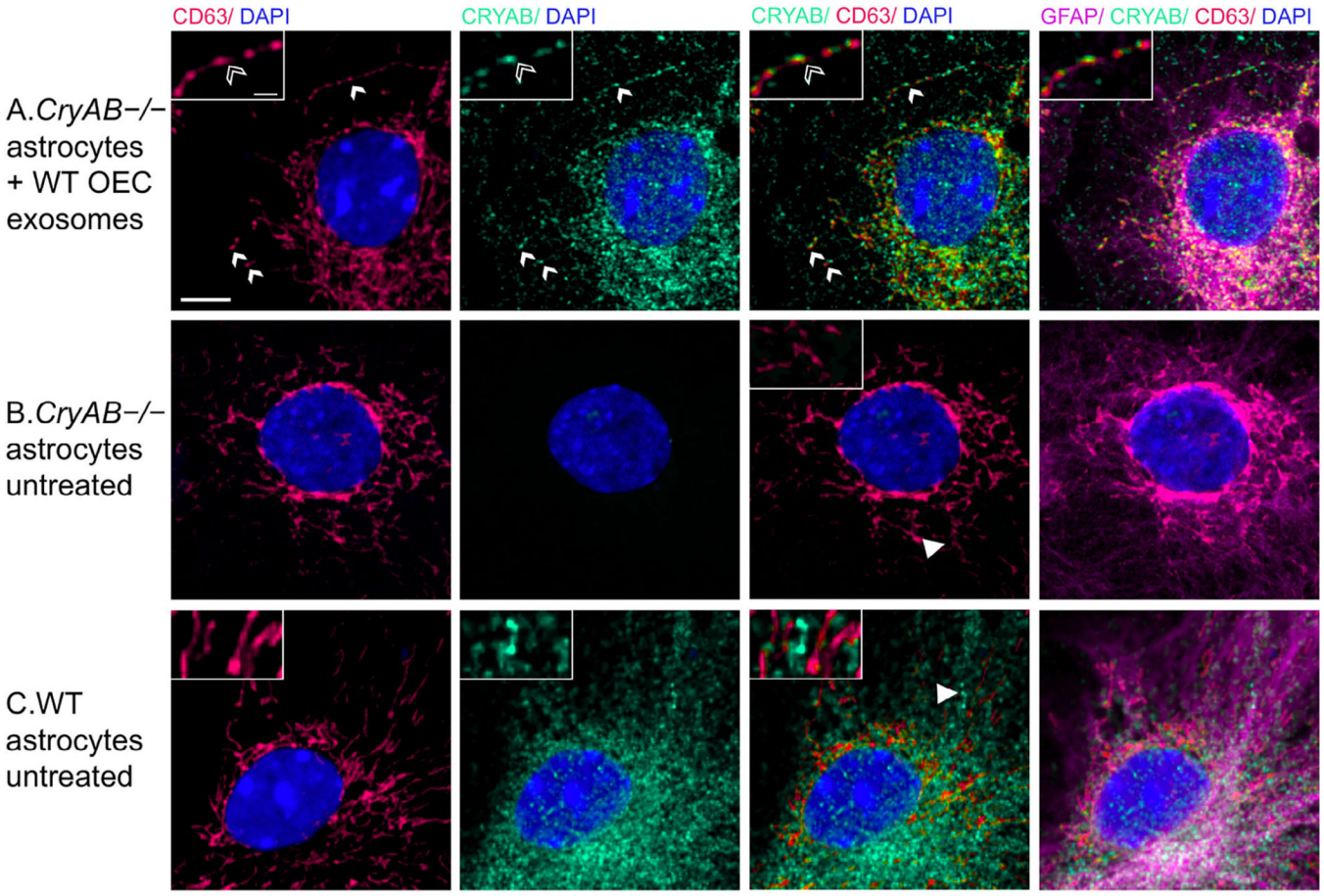

FIGURE 4.

CryAB in OEC exosomes is internalized by astrocytes. (a) OEC exosomes from WT mice were co-cultured with primary astrocytes from CryAB KO mice. (b) Untreated astrocytes from CryAB KO. (c) Untreated astrocytes from WT mice. All groups were stained for CD63 (endosomes; red), CryAB (green), GFAP (magenta), and Dapi (blue). Uptake of OEC secreted CryAB (green) is detected in $CryAB^{-/-}$ astrocytes and is often associated with endosomes (red) (A, arrows, top arrow area shown in inset, arrowhead points to CryAB positive endosome). No CryAB staining (green) is detected in untreated astrocytes from CryAB KO (B, inset). CryAB (green) is present in untreated astrocytes from WT mice but rarely associated with endosomes (C, inset, arrowhead). Scale bar represents 5 μm in low mag and 1 μm in insets

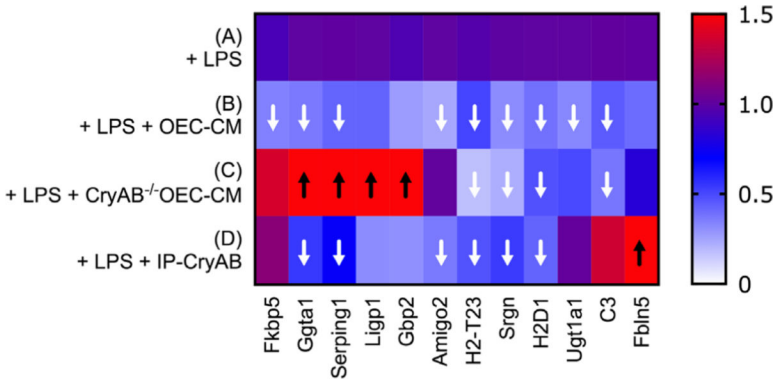

FIGURE 5.

OEC-CM suppresses multiple transcripts associated with neurotoxic astrocyte reactivity in LPS-treated astrocytes. Heat map illustrating results of Q-RT-PCR (Data S3) to detect neurotoxic astrocyte transcripts in primary astrocytes treated with LPS (A); LPS plus WT OEC-CM (B); LPS plus *CryAB*$^{-/-}$OEC-CM (C); or IP-CryAB for 24 hr (D). Compared with LPS, OEC-CM (B) significantly suppressed 9 transcripts, whereas *CryAB*$^{-/-}$OEC-CM (C) significantly suppressed 4. (D) IP-CryAB suppressed 6 of the 9 transcripts suppressed by OEC-CM. In addition, *CryAB*$^{-/-}$OEC-CM + LPS caused a significant increase in 4 transcripts, while IP-CryAB caused a significant increase in one. Finally, one transcript, C3, was significantly suppressed by both OEC-CM treatments (*CryAB*$^{-/-}$ or WT) but was elevated by IP-CryAB treatment. Q-RT-PCR experiments were analyzed by one-way ANOVA followed by Dunnett's multiple post hoc test ($n = 3$; arrows $p \leq .05$)